Shanghai Tianma Radio Telescope and Its Role in Pulsar Astronomy

Zhen Yan [1,2,*], Zhiqiang Shen [1,2], Yajun Wu [1,2], Rongbing Zhao [1,2], Jie Liu [1], Zhipeng Huang [1,2], Rui Wang [1,2], Xiaowei Wang [1,2], Qinghui Liu [1,2], Bin Li [1,2], Jinqing Wang [1,2], Weiye Zhong [1,2], Wu Jiang [1,2] and Bo Xia [1]

[1] Shanghai Astronomical Observatory, Chinese Academy of Sciences, Shanghai 200030, China; zshen@shao.ac.cn (Z.S.); wuyajun@shao.ac.cn (Y.W.); zhaorb@shao.ac.cn (R.Z.); lj@shao.ac.cn (J.L.); hzp@shao.ac.cn (Z.H.); wangrui197@shao.ac.cn (R.W.); xiaoweiwang@shao.ac.cn (X.W.); liuqinghui@shao.ac.cn (Q.L.); bing@shao.ac.cn (B.L.); jqwang@shao.ac.cn (J.W.); wyzhong@shao.ac.cn (W.Z.)

[2] School of Astronomy and Space Science, University of Chinese Academy of Sciences, Beijing 100049, China

* Correspondence: yanzhen@shao.ac.cn

Abstract: After two phases of on-site construction and testing (2010–2013 and 2013–2017), the Shanghai Tianma Radio Telescope (TMRT) can work well, with efficiencies better than 50% from 1.3 to 50.0 GHz, mainly benefiting from its low-noise cryogenic receivers and active surface system. Pulsars were chosen as important targets of research at the TMRT because of their important scientific and applied values. To meet the demands of pulsar-related observations, TMRT is equipped with some necessary backends, including a digital backend system (DIBAS) supporting normal pulsar observation modes, a real-time fast-radio-burst-monitoring backend, and baseband backends for very-long-baseline interferometry (VLBI) observations. Utilizing its high sensitivity and simultaneous dual-frequency observation capacity, a sequence of pulsar research endeavors has been undertaken, such as long-term pulsar timing, magnetar monitoring, multi-frequency (or high-frequency) observations, interstellar scintillation, pulsar VLBI, etc. In this paper, we give a short introduction about pulsar observation systems at the TMRT and briefly review the results obtained by these pulsar research projects.

1. Introduction

Pulsars are a kind of fast rotating, highly magnetized neutron star which give out lighthouse-like beams of radio emission from their magnetic poles. When a pulsar's emission beam sweeps across the Earth as it spins, we can observe a pulse. Since the discovery of the first pulsar in 1967 [1], research on pulsars has emerged as a leading and prominent subject within the realm of scientific research, and it has been thriving for a long time. About 3500 pulsars have now been discovered. There are two main classes of radio pulsars: "normal pulsars", with typical rotation periods about 0.5 s and period derivatives around 10^{-15}; and "millisecond pulsars" (MSPs), with typical periods $\leq$ 30 ms and period derivatives $\leq 10^{-19}$ [2].

The typical mass of a pulsar is about 1.44 $M_\odot$, but the radius is only about 10 km. Pulsars not only have an extremely strong gravitational field and density, comparable to atomic nuclei, but also have an exceptionally strong magnetic field, which can be up to billions of times stronger than the strongest magnetic field recorded in ground laboratories. Therefore, pulsars are regarded as natural "space laboratories" to verify the physical laws in extreme physical environments such as ultra strong gravitational fields, magnetic fields, electric fields, and at tremendously high density [3,4]. Pulsars are also important probes of the interstellar medium (ISM), as they usually show significant dispersion, interstellar scattering, interstellar scintillation, and Faraday rotation under interactions of their signals with the ISM, which can

be used to investigate the spatial distribution and fluctuation of the ISM [5,6]. Pulsars are also important tools for detecting gravitational waves in space [7–9]. In the future, the utilization of multiple millisecond pulsars (MSPs) with stable timing is anticipated for establishing "pulsar time" and improving navigation for deep space missions [10].

After more than half a century of research, significant achievements have been made using pulsars, like verifying the existence of gravitational radiation predicted by general relativity through observations of pulsar arrival times [11,12], and discovering the first exoplanet [13,14]. But, the understanding of pulsar physics is still a completely open field, as there are still various problems that need to be further solved, such as the formation process [15], physical essence [16], radiation mechanism [17], and nano-Hertz gravitational wave detection [8,9,18–22].

Due to the fact that the vast majority of pulsars only emit radiation in the radio band, radio observation is undoubtedly an important means of pulsar research. The pulsar signal is extremely weak, and statistical analysis of the 1761 pulsars with measured flux densities of 1400 MHz (S1400) shows that their S1400 distribution ranges from 0.01 to 1100 mJy, with a median of only 0.40 mJy [2]. A large-aperture telescope is indispensable for detecting such weak signals and for in-depth studies. Using the largest radio telescopes in the world, such as the Arecibo (305 m) [23], the Green Bank Telescope (100 m) [24,25], the Effelsberg (100 m) [26], the Lovell (76 m) [27], and the Parks (64 m) [28], pulsar researchers have achieved a series of important results. The newly built Five-Hundred-Meter Aperture Spherical Telescope (500 m) in China, which is the largest single-dish telescope in the world, has also become a sharp tool to obtain more and more important research results on pulsars [29–32].

The Shanghai Tianma Radio telescope (TMRT) is a newly built 65 m diameter fully-steerable radio telescope. Since the planning phase, the scientific committee of the TMRT has also chosen pulsars as one of its important research objects. In the following part of this paper, we will give a brief review of TMRT's pulsar observation systems and some interesting pulsar research results obtained with this telescope.

2. TMRT and Pulsar Observation Systems

The TMRT is jointly funded by the Chinese Academy of Sciences (CAS), Shanghai Municipality, and the Lunar Exploration Program. It is located in the rural area of Songjiang district in the southwest of Shanghai city, with the corresponding longitude and latitude of (121°08′09.121″ E, 31°05′31.031″ N) [33]. The TMRT takes its present name from a nearby small mountain named Tianma. After two phases of on-site construction and testing (2010–2013 and 2013–2017), the TMRT can work well in the frequency range from 1.3 to 50.0 GHz, taking advantages of its eight sets of low-noise cryogenic receivers and active surface system, which can effectively compensate for the surface deformation in observations [34,35]. In Figure 1, we present an aerial photograph of the TMRT taken in 2018.

The system equivalent flux density $SEFD = 2k_BT_{sys}/A_e$ is a usually used parameter to reflect the comprehensive capability of a radio telescope, as it takes both the system temperature T_{sys} and the effective aperture A_e into consideration. The majority of pulsar observations within the radio band are carried out at comparatively lower frequencies, due to their steep power-law spectra. Normally, four low-frequency receivers, which cover the frequency ranges 1.35–1.75 (L-band), 2.2–2.3 (S-band), 4.0–8.0 (C-band), and 8.2–9.0 (X-band) GHz, are usually used in pulsar observations at the TMRT. And the corresponding *SEFD* values of these four receivers are 39, 46, 30, and 48 Jy, respectively, which are comparable with other large fully steerable telescopes in the world. Especially at C-band, the TMRT has its advantages because of its wide bandwidth and low system noise [36,37].

In addition to the antenna and receiver system, a suitable backend is also very important for radio observations, as it undertakes the task of capturing the signals from receivers, making required processing, and sending the result to the recording system. Firstly, a digital backend system (DIBAS) was built for the TMRT with the kind help of the National Radio Astronomy Observatory (NRAO) to satisfy pulsar and spectral line observation

demands. The DIBAS is built by importing pulsar observation mode into the design of the Versatile GBT Astronomical Spectrometer (VEGAS), which was developed with the Collaboration for Astronomy Signal Processing and Electronics Research (CASPER) technology. For the pulsar observation modes, DIBAS can provide much the same capabilities as the Green Bank Ultimate Pulsar Processing Instrument (GUPPI) [38,39]. In Figure 2, we present the block diagram of DIBAS, which consists of three pairs of analog to digital converters (ADCs) and three corresponding Roach-II electronic boards. It supports both pulsar searching mode and online folding mode. Dedispersion is the process of reversing the effects of frequency dispersion of pulses from pulsars caused by the ISM. For incoherent dedispersion, the dispersive delays are removed by time-shifting the time series of narrow frequency channels, but there are still dispersion effects left within the channels. By comparison, coherent dedispersion is a convolution of the raw signal voltages with the inverse of the transfer function of the ISM, and can remove dispersion effects thoroughly with intensive computing [40]. Observers of the TMRT can choose the coherent or the incoherent dedispersion manner according to their demands. Graphics processing units on eight high-performance computing services are used to satisfy the intensive computation demand of the coherent dedispersion. The maximum bandwidth supported for coherent dedispersion mode is about 1 GHz, which is mostly limited by computing power. For the incoherent dedispersion observation mode, a maximum bandwidth of 6 GHz can be supported using the currently available three pairs of digitizers, as the maximum input bandwidth of each digitizer channel is up to 2 GHz. The final pulsar observation data are written out in 8-bit PSRFITS format [41]. The Lustre file system is adopted for the online observation data recording. It can satisfy the high data recording rate demand of pulsar searching observation with a time resolution as high as 40.96 µs. In addition, we also developed a real-time fast radio bursts (FRBs) monitoring backend system. In order to meet the needs of joint very-long-baseline interferometry (VLBI) observations, the Digital Base Band Converter-2 (DBBC2) system, and the Chinese VLBI Data Acquisition System (CDAS) are also equipped at the TMRT [36,37].

Figure 1. An aerial photograph of the TMRT taken in 2018. As shown in the photo, the TMRT is built in a rural area, but it is still surrounded by some villages.
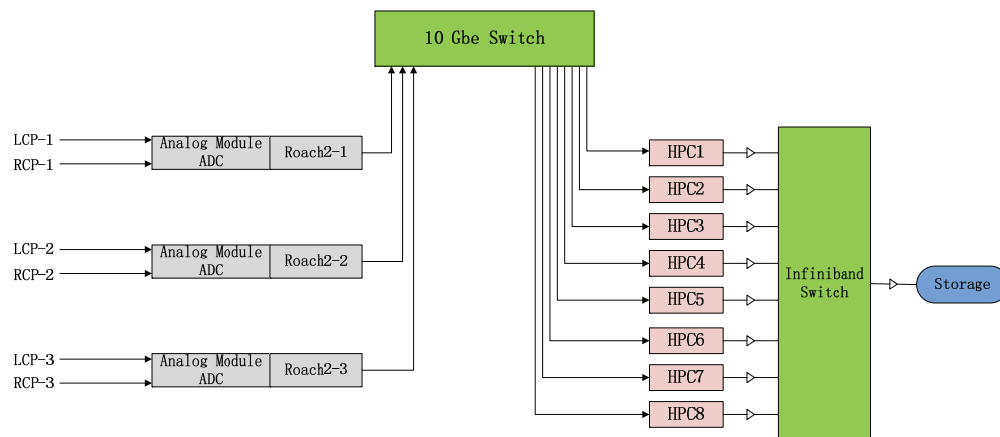
Figure 2. Block diagram of the DIBAS for the TMRT. As shown in the picture, the DIBAS mainly consists of 3 pairs of dual-polarization input interfaces, 3 pairs of analog-to-digital converters (ADCs), 3 pairs of processing Roach broads, a 10 Gbe switch, 8 high-performance computing services (HPCs), an infiniband switch, and online storage.

3. Pulsar Observation Projects and Related Results

3.1. Long-Term Pulsar Timing

Pulsar timing is the process of measuring pulses' times of arrival (TOAs) and identifying the phenomena that affect them. Accurate pulsar timing permits exquisitely sensitive measurements of quantities such as the power of gravitational radiation emitted by a pulsar in a binary system, neutron star masses, and orbital perturbations from binary companions. Based on the DIBAS backend, we have developed a stable pulsar timing observation system at the TMRT. And the long-term pulsar timing is chosen to be one of main observation projects of this telescope. We regularly monitor timing properties of about 350 pulsars at S-band (or C-band). For some millisecond pulsars, we can achieve a timing accuracy better than sub-microsecond. In Figure 3, we present the timing observation results of a millisecond pulsar J1909-3744 at C-band. It can be seen that the root mean square (RMS) of our observations on this pulsar is about 0.170 μs.
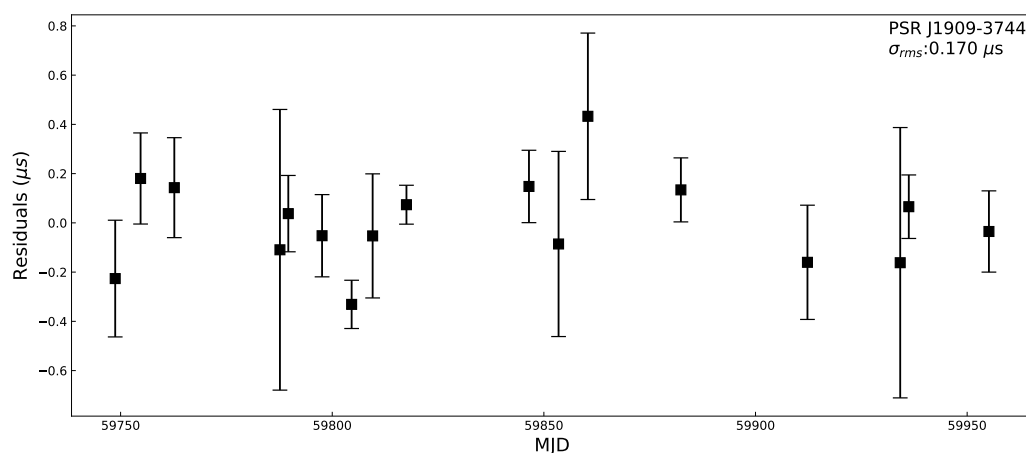

Figure 3. PSR J1909-3744 timing observation results obtained with the TMRT at C-band. The central frequency and bandwidth of these observations are 4.75 GHz and 1.0 GHz, respectively. The typical integration length for each point is about 2–4 h.

A series of interesting findings has been derived from the extensive analysis of long-term pulsar timing data acquired with the TMRT. One large glitch of PSR B1737-30 around MJD 58,232.4 was reported based on timing observation data from MJD 57,999 to 58,406 at the S-band. It was found that this pulsar underwent an increase in the rotation frequency ($\Delta\nu$) of about 1.38×10^{-6} Hz, corresponding to a fractional step change in $\Delta\nu/\nu$ of $\sim 8.39 \times 10^{-7}$.

Compared with its 36 glitches reported since July 1987, this glitch ranked the fourth largest one among historical results. It was also found that the glitch size distribution could be well described by a power-law with the index of 1.13, and the distribution of the interval between two adjacent glitches was found to follow a Poissonian probability density function [42]. Although there were not any glitch reports about PSR B2021+51, its glitch was firstly detected at the TMRT using timing observation data from MJD 57,640 to 58,842. Affected by the glitch occurring around MJD 58,289.1, the spin frequency (ν), and its derivative ($\dot{\nu}$), of PSR B2021+51 suffered jumps of about 7.04×10^{-10} Hz and 2.6×10^{-18} s^{-2}, respectively. What is even more interesting is that the W10 (width of the mean pulse at 10% of the maximum height) of this pulsar significantly decreased right before the glitch, and then, increased immediately after the glitch. According to further analyses on three decomposed Gaussian components (C1, C2, and C3 from left to right by peak phase) of its mean pulse profiles, the corresponding profile changes were explained by relative component movements. This also gives us some clues about a potential connection between the changes in characteristics of the pulsar emission zone and the glitch activity [43].

3.2. Magnetar Monitoring

Magnetars are a sub-group of neutron stars with extremely strong magnetic fields ($B \sim 10^{13}$–10^{15} G). They sometimes show extremely strong X-ray or γ-ray bursts which are not possible by losing rotational energy as for ordinary pulsars, so it is widely thought that their radiation derives energy from the decay of magnetic fields [44]. Meanwhile, magnetars also have longer rotation periods ($P \sim 1$–12 s) and show more irregular rotations than ordinary pulsars [45,46]. To date, the identification of magnetars and potential candidates remains limited, with only 32 instances documented so far. Among these, merely six magnetars have exhibited detectable radio pulsations [47].

The history of magnetar observations at the TMRT can be traced back to the early stages of the second phase of its construction. SGR J1745-2900 is a magnetar detected near the galactic center from its outburst activity starting on MJD 56,408 (26 April 2013) [48]. Six epochs of observation on this interesting source were arranged at 8.60 GHz between June and October, 2014, at the TMRT. As both the flux density and integrated profile of PSR J1745-2900 showed dramatic changes from epoch to epoch, these findings further confirmed that this magnetar was still in the "erratic" phase. The flux density of this magnetar was found to be about 8.7 mJy on MJD 56,836, which was about 10 times stronger than that at the discovery. Its emission was reported to be dominated by narrow ("spiky") pulses that follow a log-normal distribution in peak flux density. Based on further total energy analyses, it was confirmed that the bright spiky pulses could not be classified as usual "giant" pulses, because their total energies did not exceed 10 times that of the integrated profile. Compared with the giant pulses, no clear correlation was found between the widths and peak flux densities of these bright spiky pulses [39]. This research work was the prelude to performing magnetar and pulsar studies with the TMRT.

Swift J1818.0-1607 is a new radio-loud magnetar discovered by the Swift Burst Alert Telescope on 12 March 2020 [49,50]. Long-term (from MJD 58,936 to 59,092) dual-frequency monitoring on this interesting source was arranged by taking advantage of the simultaneous 2.25/8.60 GHz working ability of the TMRT. By comparison, few multi-frequency observations had been carried out on this magnetar previously. These dual-frequency observations gave valuable information about how its integrated profiles and flux densities changed with both time and frequency. Its flux densities were found to increase at both 2.25 and 8.60 GHz, accompanying the spectra getting flatter. Because of its instable integrated profiles and timing properties, the ν and $\dot{\nu}$ were obtained with the piece-wise fitting method, in which the long-term timing observations were separated into multiple segments. The length of each segment lasted until there was obvious changes in the integrated profiles or the error or fitted $\dot{\nu}$ exceeded 2.70×10^{-12} s^{-2}, which was about 10% of the mean $\dot{\nu}$ [51]. Based on the long-term declining trend result of ν fitted with observational data spanning a much longer period than previous works, a more accurate characteristic age (τ) of

this magnetar was found to be about 522 yr. And this result gave further support to the viewpoint that this magnetar may be older than initially thought at the time of discovery ($\tau \sim 240$ yr) [52]. Furthermore, Swift J1818.0-1607 was found to synchronously switch between the bright and quiet (B-Q) emission modes at 2.25 and 8.60 GHz over three days of TMRT observations [53].

After spending almost a decade in a radio-quiet state, the magnetar XTE J1810-197 turned back on in early December 2018 [54,55]. In order to study its rotation and radiation properties, simultaneous 2.25/8.60 GHz observations of XTE J1810-197 were frequently arranged at the TMRT. Based on the results from 194 epochs of observation in the following 926 days, it was found that the integrated profiles of XTE J1810-197 could be classified into 12 types according to phase areas of active radiation components, although they changed obviously with the time and frequency during this period. In addition to the short-term ν and $\dot{\nu}$ results obtained with the piece-wise fitting method, a long-term declining trend in ν was also obtained as $\dot{\nu} = -3.2(1) \times 10^{-13}$ s^{-2} with the linear fitting method. XTE J1810-197 was found to show a relatively flat spectrum ($\alpha > -1$) in most of observations. The emission heights of XTE J1810-197 at 2.25 and 8.60 GHz were about $7.5(9) \times 10^4$ km and $2.38(7) \times 10^4$ km, respectively, assuming an ideal dipole magnetic field [56].

3.3. Multi-Frequency (or High-Frequency) Observations and Pulsar Radiation

The pulsar radiation process remains an open field. Various theoretical models have been posited about beam patterns of pulsars, including but not limited to the core–cone [57], patchy [58], and fan beam [59] models. The "radius-to-frequency mapping" (RFM) model specifies that emissions at different frequencies are produced at different altitudes in the pulsar magnetosphere. The observations of the mean (average) pulse profile gives us insight into long-term statistical properties of the processes ongoing in a pulsar magnetosphere, while the observations of individual pulses give us insight into its momentary state [60].

Taking advantage of its comparatively high sensitivity and dual-frequency observation ability, a series of research projects about pulsar radiation were arranged at the TMRT. In addition to the integrated pulse profiles at 8.6 GHz for a sample of 26 pulsars obtained with the TMRT, their mean flux densities and pulse width parameters were also estimated. For 11 of the pulsars these were the first high-frequency observations, and for a further 4 they had better signal-to-noise ratios (SNRs) than previous observations [61]. In addition, integrated pulse profiles at 5 GHz for 63 normal pulsars and 8 millisecond pulsars (MSPs) were obtained using the TMRT. Meanwhile, their flux densities and pulse widths were also measured. For 19 normal pulsars and 1 MSP, these were the first detections at 5 GHz, and for a further 19 pulsars (including 5 MPSs) they had better SNR profiles than previous observations. Correlations of power-law spectral index were found with characteristic age, radio pseudo-luminosity, and spin-down luminosity [62]. The frequency dependence of component separations was also investigated, and three groups were found: the separation between the outmost leading and trailing components decreased with the frequency (50%), roughly in agreement with radius-to-frequency mapping; the separations were nearly constant (50%); the separation between the outmost components increased with the frequency (the remaining few).

Benefiting from the simultaneous dual-frequency observation ability, a mutual timing calibration technique was proposed and tested on 2.25 and 8.60 GHz observations. It was attempted to effectively extend the total integration length for 8.60 GHz observations by using timing solutions obtained from observation results at 2.25 GHz because of their sufficient SNRs for timing analyses. In order to give a direct answer about whether it was possible to obtain reliable integrated profiles by coherently adding observation data spanning tens of days, observations with the same mode were also arranged on PSR B0355+54, a technical verification source, which was a strong normal pulsar easily detected in each epoch of observation at both 2.25 and 8.60 GHz [63]. Figure 4 displays the integrated profiles of PSR B0355+54 obtained from a single epoch of 10.1 h observation (on MJD 59,209), along with the integrated profiles generated by summing observation

data from MJDs 58,915 to 59,418 (except the observation on MJD 59,209). It is clear that there are no evident differences between them, giving strong support to these related techniques. Using this technique, it was possible to present the detection results of nine MSPs at 8.60 GHz, which significantly increased the number of MSPs with published profiles (from four to eleven) above 8.0 GHz, as seven of our target MSPs had no related results previously. The spectra of four MSPs (J1012-5307, J1022+1001, J1713+0747, and J2145-0750) were found to deviate from a single power-law, and a broken power-law was used to fit these results. Furthermore, the profile changes of PSR J1713+0747, which started around MJDs 59,320–59,321 [64], were found to be more prominent as the observation frequency became higher (see Figure 5), so the models of some changes in the magnetosphere were preferred to explain this event in comparison with models of the interstellar medium effects [65]. Additionally, pulsar radio radiation models (especially the inverse Compton scattering model) were studied grounded in analyses of multi-frequency observation results spanning a wider frequency range [66,67].
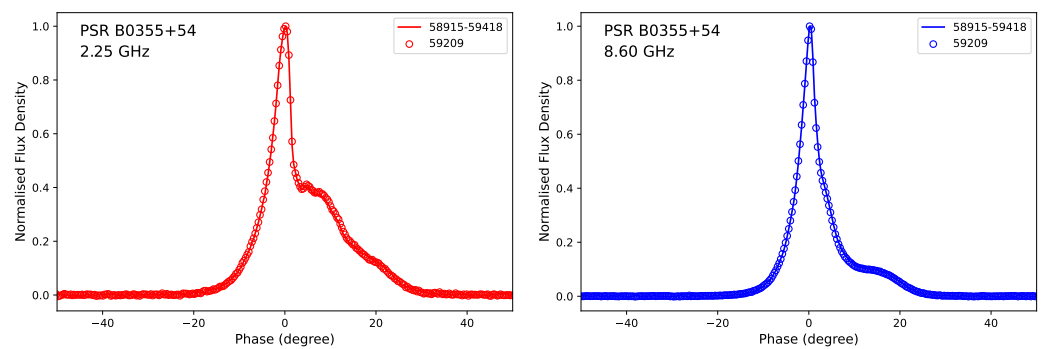

Figure 4. Integrated profiles of PSR B0355+54 at 2.25 (**left**) and 8.60 GHz (**right**). In each panel, the hollow dot line is the integrated profile from the observation on MJD 59,029, and the solid line represents the integrated profile obtained from observations between MJDs 58,915 and 59,418 (the observation on MJD 59,029 is excluded).
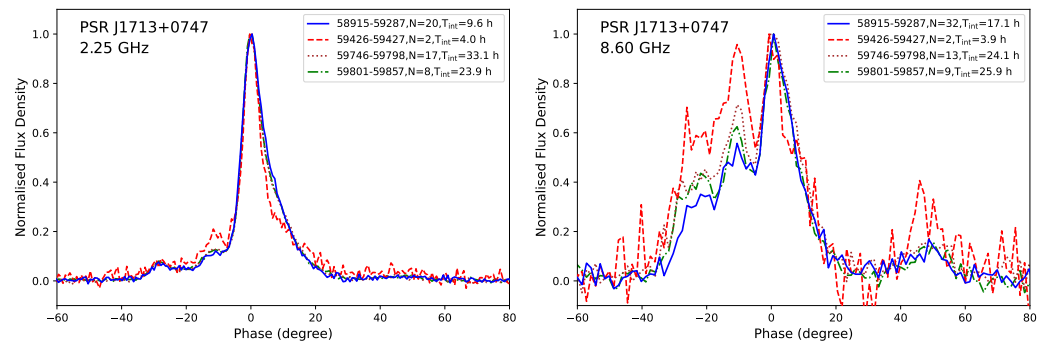

Figure 5. The integrated profiles of PSR J1713+0747 before (blue line) and after (red dashed, brown dotted and green dash–dot line) the profile change event. The 2.25 and 8.60 GHz observation results are shown in the left and right sub-panels, respectively. For easier comparison, each integrated profile is normalized with the corresponding peak flux density.

In addition, there was also a series of single-pulse observations arranged to study related momentary properties. The mode-changing properties of PSR B0329+54 were investigated using 31 epochs of simultaneous 2.25/8.60 GHz single-pulse observations obtained with the TMRT. The pulsar was found to be in the abnormal emission mode 17 times, accounting for about 13% of the 41.6 h total observation time. Single-pulse analyses indicated that mode changes took place simultaneously at 2.25/8.60 GHz within a few rotational periods. Occasional bright narrow pulses, which appeared as peak flux densities 10 times higher than that of the integrated profile, were detected at both frequencies. The total energy of these pulses was not so large as a "giant" pulse, so these pulses could be

classified as the "spiky" pulses of PSR B0656+14 [68]. The detection rate of these spiky pulses at 8.60 GHz was tens of times higher than that at 2.25 GHz, which could by caused by the fact that higher-frequency emissions came from the more active area at a lower altitude in the pulsar magnetosphere. By dividing the pulsar radiation window into three components (C1, C2, and C3), corresponding to the main peaks of the integrated profile, and giving further analysis with the two-dimensional fluctuation spectrum (2DFS), C3 was found to have a stronger quasi-periodic modulation centered around 0.06 cycles/period in the abnormal mode at 8.60 GHz, while no similar phenomenon was detected in the simultaneous 2.25 GHz observations [69]. The bright pulses from PSR B0031-07 were detected at 4820 MHz and found to repeat in an irregular fashion, as the intervals between these bright pulses could be described with an exponentiated Weibull distribution [70].

4. Pulsar Interstellar Scintillation Observations

Normally, the luminosity of pulsars maintains intrinsic stability over time scales ranging from a few hours to several years [71]. For a such a compact source with stable flux density, it will scintillate when its radio radiation pass the inhomogeneous interstellar medium, especially at relatively lower frequencies. Pulsar scintillation is similar to the twinkling, or scintillation, of stars due to the Earth's turbulent atmosphere. The observation of pulsars' scintillation can be used to probe both the distribution and fluctuation of the interstellar medium [5,72,73]. Currently, a pulsar interstellar scintillation observation project is being carried out at the TMRT. In Figure 6, we give a sample of dynamic spectrum plots for interstellar scintillation observations on PSRs B0144+59 and B0450+55 at 2.25 GHz. It is clear that obvious diffractive interstellar scintillation phenomena have been detected. Further observations and data analyses are to be carried out, and some more interesting results will be reported in the near future.
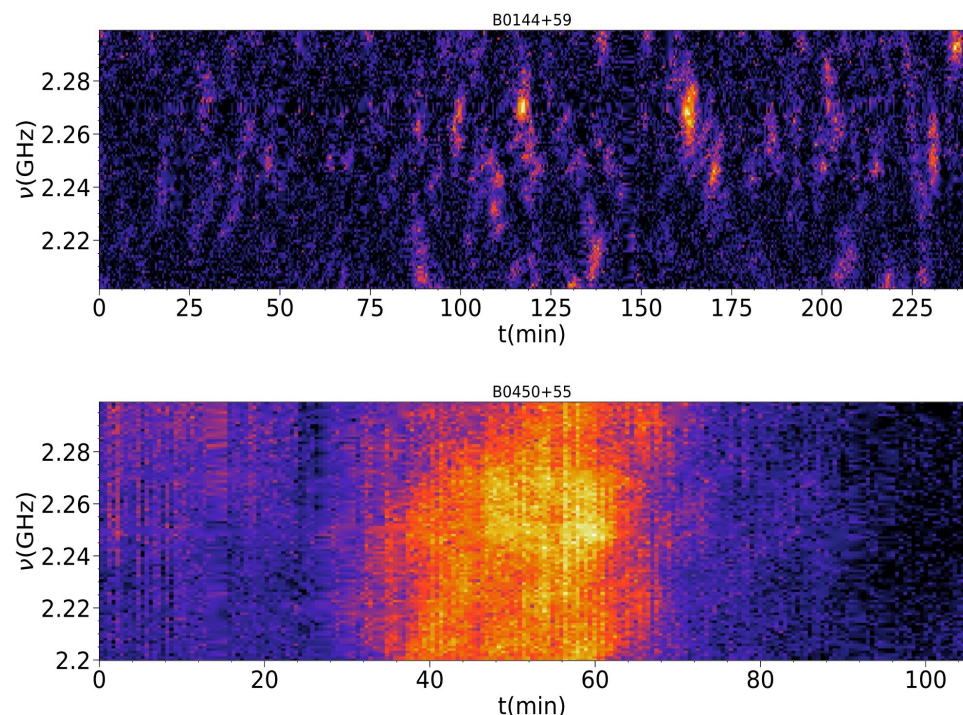

Figure 6. Dynamic spectrum plots for interstellar scintillation observations on PSRs B0144+59 (**top**) and B0450+55 (**bottom**) at 2.25 GHz. The observed flux density of the corresponding pulsar is linearly scaled with the brightness of the corresponding pixel.

5. Pulsar VLBI Observations

Accurate distance and proper motion measurements of a pulsar are important for fundamental astrophysical questions, such as supernova explosion kicks, the equations of

state of neutron stars, and the galactic electron density distribution. Though it is possible to fit pulsars' distances and proper motions with high-sensitivity pulsar timing observations, this is applicable for pulsars with comparatively stable timing properties. High-precision VLBI astrometry offers a powerful way to directly measure the parallaxes and proper motions of pulsars. Compared with pulsar timing, the pulsar astrometry with the VLBI only needs to fit five parameters. Pathfinding pulsar astrometry with short-baseline radio interferometry started in the 1970s [74,75]. By the steady progress of the VLBI observation, correlation, and data processing techniques, the astrometry parameters of tens of pulsars have been obtained with the VLBI [76–80].

The TMRT has become a significant constituent within some VLBI networks, such as the Chinese VLBI Network (CVN), European VLBI Network (EVN), and East Asia VLBI Network (EAVN), and has performed some pulsar observations with them. In addition, there were some pathfinder observations with TMRT plus the VLBA also arranged. The partition of the TMRT lengthened the projected baseline in the east–west direction by a factor of two and makes the UV coverage of observation much better for pulsars located at high declinations. In Figure 7, we present an image of PSR B0458+46 obtained with TMRT plus the VLBA at L-band, and its position can be obtained with an accuracy better than a milliarcsecond (mas). More VLBI pulsar observation results including the TMRT are being processed.
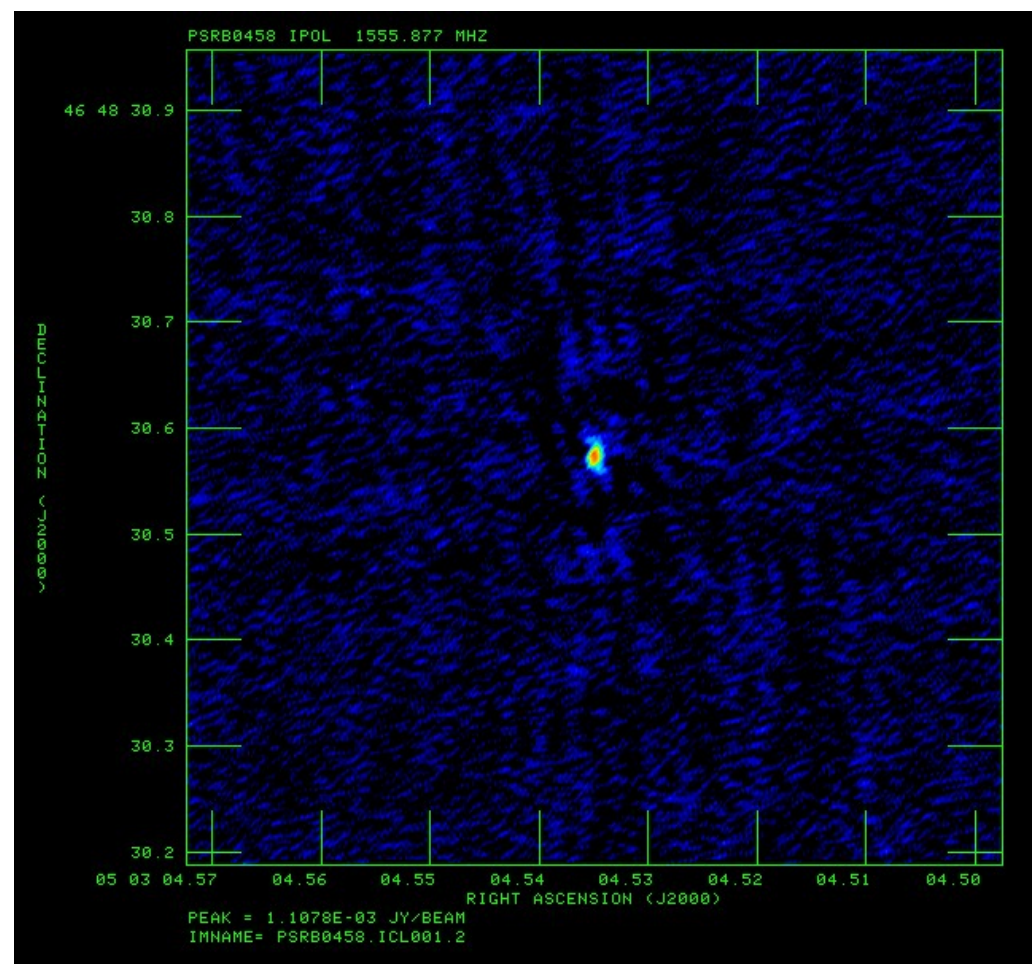

Figure 7. An image of PSR B0458+46 obtained with TMRT plus the VLBA at L-band. The effective integration length on the target pulsar was about 80 min.

6. Conclusions

Pulsars were chosen as one of the important scientific research objects of the newly built TMRT, and some interesting observation results have been obtained. In addition, there are also some other pulsar-related research projects, such as deep pulsar hunting around the galactic center at high frequency, and fast radio bursts monitoring, being carried out at this telescope. It can be predicted that more and more interesting research achievements about pulsars will be made with the TMRT.

Author Contributions: Conceptualization, methodology, and project administration: Z.Y. and Z.S. data reduction and investigation: J.L., Z.H., R.W. and X.W.; software and hardware: Y.W., R.Z., Q.L., B.L., J.W., W.Z., W.J. and B.X.; writing—original draft preparation: Z.Y.; writing—review and editing: other authors. All authors have read and agreed to the published version of the manuscript.

Data Availability Statement: The data underlying this article will be shared on reasonable request to the corresponding author.

Conflicts of Interest: The authors declare no conflicts of interest.

List of Abbreviations

Abbreviation	Meaning
MSP	Millisecond pulsar
S1400	Flux density at 1400 MHz
TMRT	Tianma Radio Telescope
SEFD	System equivalent flux density
DIBAS	Digital backend system
NRAO	National Radio Astronomy Observatory
GBT	Green Bank Telescope
VEGAS	Versatile GBT Astronomical Spectrometer
CASPER	Collaboration for Astronomy Signal Processing and Electronics Research
GUPPI	Green Bank Ultimate Pulsar Processing Instrument
ADC	Analog-to-digital converter
HPC	High-performance computing
FRB	Fast radio burst
VLBI	Very-long-baseline interferometry
DBBC2	Digital Base Band Converter-2
CDAS	Chinese VLBI Data Acquisition System
PSRFITS	Pulsar data format based on flexible image transport system
TOAs	Pulse times of arrival
RFM	Radius-to-frequency mapping
SNR	Signal-to-noise ratio
2DFS	Two-dimensional fluctuation spectrum
CVN	Chinese VLBI Network
EVN	European VLBI Network
EAVN	East Asia VLBI Network

References

1. Hewish, A.; Bell, S.J.; Pilkington, J.D.H.; Scott, P.F.; Collins, R.A. Observation of a Rapidly Pulsating Radio Source. *Nature* **1968**, *217*, 709–713. [CrossRef]
2. Manchester, R.N.; Hobbs, G.B.; Teoh, A.; Hobbs, M. The Australia Telescope National Facility Pulsar Catalogue. *Astron. J.* **2005**, *129*, 1993–2006. [CrossRef]

3. Cordes, J.; Kramer, M.; Lazio, T.; Stappers, B.; Backer, D.; Johnston, S. Pulsars as tools for fundamental physics & astrophysics. *New Astron. Rev.* **2004**, *48*, 1413–1438.

4. Xu, R.X. Pulsars and Quark Stars. *Chin. J. Astron. Astrophys.* **2006**, *6*, 279–286. [CrossRef]

5. Rickett, B.J. Radio Propagation through the Turbulent Interstellar Plasma. *Annu. Rev. Astron. Astrophys.* **1990**, *28*, 561–605. [CrossRef]

6. Han, J.L.; Manchester, R.N.; Lyne, A.G.; Qiao, G.J.; van Straten, W. Pulsar rotation measures and the large-scale structure of the Galactic magnetic field. *Astrophys. J.* **2006**, *642*, 868–881. [CrossRef]

7. Reardon, D.J.; Zic, A.; Shannon, R.M.; Hobbs, G.B.; Bailes, M.; Di Marco, V.; Kapur, A.; Rogers, A.F.; Thrane, E.; Askew, J.; et al. Search for an Isotropic Gravitational-wave Background with the Parkes Pulsar Timing Array. *Astrophys. J. Lett.* **2023**, *951*, L6. [CrossRef]

8. Agazie, G.; Anumarlapudi, A.; Archibald, A.M.; Arzoumanian, Z.; Baker, P.T.; Bécsy, B.; Blecha, L.; Brazier, A.; Brook, P.R.; Burke-Spolaor, S.; et al. The NANOGrav 15 yr Data Set: Evidence for a Gravitational-wave Background. *Astrophys. J. Lett.* **2023**, *951*, L8. [CrossRef]

9. Xu, H.; Chen, S.; Guo, Y.; Jiang, J.; Wang, B.; Xu, J.; Xue, Z.; Nicolas Caballero, R.; Yuan, J.; Xu, Y.; et al. Searching for the Nano-Hertz Stochastic Gravitational Wave Background with the Chinese Pulsar Timing Array Data Release I. *Res. Astron. Astrophys.* **2023**, *23*, 075024. [CrossRef]

10. Hobbs, G.; Coles, W.; Manchester, R.N.; Keith, M.J.; Shannon, R.M.; Chen, D.; Bailes, M.; Bhat, N.D.R.; Burke-Spolaor, S.; Champion, D.; et al. Development of a pulsar-based timescale. *Mon. Not. R. Astron. Soc.* **2012**, *427*, 2780–2787. [CrossRef]

11. Hulse, R.A.; Taylor, J.H. Discovery of a pulsar in a binary system. *Astrophys. J. Lett.* **1975**, *195*, L51–L53. [CrossRef]

12. Taylor, J.H., Jr. Binary pulsars and relativistic gravity. *Rev. Mod. Phys.* **1994**, *66*, 711–719. [CrossRef]

13. Wolszczan, A.; Frail, D.A. A planetary system around the millisecond pulsar PSR1257 + 12. *Nature* **1992**, *355*, 145–147. [CrossRef]

14. Mayor, M.; Queloz, D. A Jupiter-mass companion to a solar-type star. *Nature* **1995**, *378*, 355–359 [CrossRef]

15. Faucher-Giguère, C.A.; Kaspi, V.M. Birth and Evolution of Isolated Radio Pulsars. *Astrophys. J.* **2006**, *643*, 332–355. [CrossRef]

16. Lattimer, J.M.; Prakash, M. The Physics of Neutron Stars. *Science* **2004**, *304*, 536–542. [CrossRef] [PubMed]

17. Philippov, A.; Kramer, M. Pulsar Magnetospheres and Their Radiation. *Annu. Rev. Astron. Astrophys.* **2022**, *60*, 495–558. [CrossRef]

18. Manchester, R.N. Observational Properties of Pulsars. *Science* **2004**, *304*, 542–547. [CrossRef]

19. Lorimer, D.R. Binary and Millisecond Pulsars. *Living Rev. Relativ.* **2008**, *11*, 8. [CrossRef]

20. Beskin, V.S. Radio pulsars: Already fifty years! *Phys. Uspekhi* **2018**, *61*, 353–380. [CrossRef]

21. Zic, A.; Reardon, D.J.; Kapur, A.; Hobbs, G.; Mandow, R.; Curyło, M.; Shannon, R.M.; Askew, J.; Bailes, M.; Bhat, N.D.R.; et al. The Parkes Pulsar Timing Array third data release. *Publ. Astron. Soc. Aust.* **2023**, *40*, e049. [CrossRef]

22. Antoniadis, J.; Arumugam, P.; Arumugam, S.; Babak, S.; Bagchi, M.; Bak Nielsen, A.S.; Bassa, C.G.; Bathula, A.; Berthereau, A.; Bonetti, M.; et al. [EPTA Collaboration; InPTA Collaboration]. The second data release from the European Pulsar Timing Array. III. Search for gravitational wave signals. *Astron. Astrophys.* **2023**, *678*, A50.

23. Altschuler, D.R.; Salter, C.J. The Arecibo Observatory: Fifty astronomical years. *Phys. Today* **2013**, *66*, 43. [CrossRef]

24. Ransom, S.M. Pulsars in Globular Clusters. In *Proceedings of the Dynamical Evolution of Dense Stellar Systems*; Vesperini, E., Giersz, M., Sills, A., Eds.; Cambridge University Press: Cambridge, UK, 2008; Volume 246, pp. 291–300.

25. Lynch, R.S. The Green Bank North Celestial Cap Pulsar Survey: Status and Future. In *Proceedings of the Pulsar Astrophysics the Next Fifty Years*; Weltevrede, P., Perera, B.B.P., Preston, L.L., Sanidas, S., Eds.; Cambridge University Press: Cambridge, UK, 2018; Volume 337, pp. 13–16.

26. Barr, E.D.; Champion, D.J.; Kramer, M.; Eatough, R.P.; Freire, P.C.C.; Karuppusamy, R.; Lee, K.J.; Verbiest, J.P.W.; Bassa, C.G.; Lyne, A.G.; et al. The Northern High Time Resolution Universe pulsar survey-I. Setup and initial discoveries. *Mon. Not. R. Astron. Soc.* **2013**, *435*, 2234–2245. [CrossRef]

27. Lyne, A.; Morison, I. The Lovell Telescope and its role in pulsar astronomy. *Nat. Astron.* **2017**, *1*, 835–840. [CrossRef]

28. Manchester, R.N.; Lyne, A.G.; Camilo, F.; Bell, J.F.; Kaspi, V.M.; D'Amico, N.; McKay, N.P.F.; Crawford, F.; Stairs, I.H.; Possenti, A.; et al. The Parkes multi-beam pulsar survey-I. Observing and data analysis systems, discovery and timing of 100 pulsars. *Mon. Not. R. Astron. Soc.* **2001**, *328*, 17–35.

29. Jiang, P.; Tang, N.Y.; Hou, L.G.; Liu, M.T.; Krčo, M.; Qian, L.; Sun, J.H.; Ching, T.C.; Liu, B.; Duan, Y.; et al. The fundamental performance of FAST with 19-beam receiver at L band. *Res. Astron. Astrophys.* **2020**, *20*, 064. [CrossRef]

30. Li, D.; Dickey, J.M.; Liu, S. Preface: Planning the scientific applications of the Five-hundred-meter Aperture Spherical radio Telescope. *Res. Astron. Astrophys.* **2019**, *19*, 016. [CrossRef]

31. Han, J.L.; Wang, C.; Wang, P.F.; Wang, T.; Zhou, D.J.; Sun, J.H.; Yan, Y.; Su, W.Q.; Jing, W.C.; Chen, X.; et al. The FAST Galactic Plane Pulsar Snapshot survey: I. Project design and pulsar discoveries. *Res. Astron. Astrophys.* **2021**, *21*, 107. [CrossRef]

32. Pan, Z.; Qian, L.; Ma, X.; Liu, K.; Wang, L.; Luo, J.; Yan, Z.; Ransom, S.; Lorimer, D.; Li, D.; et al. FAST Globular Cluster Pulsar Survey: Twenty-four Pulsars Discovered in 15 Globular Clusters. *Astrophys. J. Lett.* **2021**, *915*, L28. [CrossRef]

33. Li, J.; Xiong, F.; Yu, C.; Zhang, J.; Guo, L.; Fan, Q. Precise determination of the reference point coordinates of Shanghai Tianma 65-m radio telescope. *Chin. Sci. Bull.* **2014**, *59*, 2558–2567. [CrossRef]

34. Wang, J.; Zuo, X.; Michael, K.; Zhao, R.; Yu, L.; Jiang, Y.; Gou, W.; Jiang, Y.; Guo, W. TM65 m radio telescope microwave holography. *Sci. Sin. Phys. Mech. Astron*. **2017**, *47*, 099502. [CrossRef]

35. Dong, J.; Fu, L.; Liu, Q.; Shen, Z. Measuring and analyzing thermal deformations of the primary reflector of the Tianma radio telescope. *Exp. Astron.* **2018**, *45*, 397–410. [CrossRef]

36. Yan, Z.; Shen, Z.Q.; Wu, Y.J.; Zhao, R.B.; Liu, Q.H. Pulsar studies with Shanghai tian ma radio telescope. In Proceedings of the 2017 XXXIInd General Assembly and Scientific Symposium of the International Union of Radio Science (URSI GASS), Montreal, QC, Canada, 19–26 August 2017; IEEE: Piscataway, NJ, USA, 2017; pp. 1–4.

37. Yan, Z.; Shen, Z.Q.; Wu, Y.J.; Zhao, R.B.; Zhao, R.S.; Liu, J.; Huang, Z.P.; Liu, Q.H.; Wu, X.J. Pulsar research with the newly built Shanghai tian ma radio telescope. *URSI Radio Sci. Bull.* **2018**, *2018*, 10–18.

38. Prestage, R.M.; Bloss, M.; Brandt, J.; Creager, R.; Demorest, P.; Ford, J.; Jones, G.; Luo, J.; McCullough, R.; Ransom, S.M.; et al. Experiences with the Design and Construction of Astronomical Instrumentation using CASPER: The Digital Backend System. In *American Astronomical Society Meeting Abstracts #223;* The American Astronomical Society: Washington, DC, USA, 2014; Volume 223, p. 148.30.

39. Yan, Z.; Shen, Z.Q.; Wu, X.J.; Manchester, R.N.; Weltevrede, P.; Wu, Y.J.; Zhao, R.B.; Yuan, J.P.; Lee, K.J.; Fan, Q.Y.; et al. Single-pulse Radio Observations of the Galactic Center Magnetar PSR J1745-2900. *Astrophys. J.* **2015**, *814*, 5. [CrossRef]

40. Hankins, T.H. Coherent Dedispersion: History and Results. In *Proceedings of the Pulsar Astrophysics the Next Fifty Years;* Weltevrede, P., Perera, B.B.P., Preston, L.L., Sanidas, S., Eds.; Cambridge University Press: Cambridge, UK, 2018; Volume 337, pp. 29–32.

41. Hotan, A.W.; van Straten, W.; Manchester, R.N. PSRCHIVE and PSRFITS: An Open Approach to Radio Pulsar Data Storage and Analysis. *Publ. Astron. Soc. Aust.* **2004**, *21*, 302–309. [CrossRef]

42. Liu, J.; Yan, Z.; Yuan, J.P.; Zhao, R.S.; Huang, Z.P.; Wu, X.J.; Wang, N.; Shen, Z.Q. One large glitch in PSR B1737-30 detected with the TMRT. *Res. Astron. Astrophys.* **2019**, *19*, 073. [CrossRef]

43. Liu, J.; Wang, H.G.; Yan, Z.; Shen, Z.Q.; Tong, H.; Huang, Z.P.; Zhao, R.S. Pulse Profile Variations Associated with the Glitch of PSR B2021+51. *Astrophys. J.* **2021**, *912*, 58. [CrossRef]

44. Damour, T.; Taylor, J.H. Strong–Field Tests of Relativistic Gravity and Binary Pulsars. *Phys. Rev. D* **1992**, *45*, 1840–1868. [CrossRef]

45. Tong, H.; Xu, R.X.; Song, L.M.; Qiao, G.J. Wind Braking of Magnetars. *Astrophys. J.* **2013**, *768*, 144. [CrossRef]

46. Gao, Z.F.; Li, X.D.; Wang, N.; Yuan, J.P.; Wang, P.; Peng, Q.H.; Du, Y.J. Constraining the braking indices of magnetars. *Mon. Not. R. Astron. Soc.* **2016**, *456*, 55–65. [CrossRef]

47. Olausen, S.A.; Kaspi, V.M. The McGill Magnetar Catalog. *Astrophys. J. Suppl. Ser.* **2014**, *212*, 6. [CrossRef]

48. Karuppusamy, R.; Stappers, B.W.; Serylak, M. A low frequency study of PSRs B1133+16, B1112+50, and B0031-07. *Astron. Astrophys.* **2011**, *525*, A55. [CrossRef]

49. Enoto, T.; Sakamoto, T.; Younes, G.; Hu, C.P.; Ho, W.C.G.; Gendreau, K.; Arzoumanian, Z.; Guver, T.; Guillot, S.; Altamirano, D.; et al. NICER detection of 1.36 sec periodicity from a new magnetar, Swift J1818.0-1607. *Astron. Telegr.* **2020**, *13551*, 1.

50. Esposito, P.; Rea, N.; Borghese, A.; Coti Zelati, F.; Viganò, D.; Israel, G.L.; Tiengo, A.; Ridolfi, A.; Possenti, A.; Burgay, M.; et al. A Very Young Radio-loud Magnetar. *Astrophys. J. Lett.* **2020**, *896*, L30. [CrossRef]

51. Champion, D.; Cognard, I.; Cruces, M.; Desvignes, G.; Jankowski, F.; Karuppusamy, R.; Keith, M.J.; Kouveliotou, C.; Kramer, M.; Liu, K.; et al. High-cadence observations and variable spin behaviour of magnetar Swift J1818.0-1607 after its outburst. *Mon. Not. R. Astron. Soc.* **2020**, *498*, 6044–6056. [CrossRef]

52. Hu, C.P.; Strohmayer, T.E.; Ray, P.S.; Enoto, T.; Guver, T.; Guillot, S.; Jaisawal, G.K.; Younes, G.; Gendreau, K.; Arzoumanian, Z.; et al. NICER follow-up observation and a candidate timing anomaly from Swift J1818.0-1607. *Astron. Telegr.* **2020**, *13588*, 1.

53. Huang, Z.P.; Yan, Z.; Shen, Z.Q.; Tong, H.; Lin, L.; Yuan, J.P.; Liu, J.; Zhao, R.S.; Ge, M.Y.; Wang, R. Simultaneous 2.25/8.60 GHz observations of the newly discovered magnetar-Swift J1818.0-1607. *Mon. Not. R. Astron. Soc.* **2021**, *505*, 1311–1315. [CrossRef]

54. Gotthelf, E.V.; Halpern, J.P.; Alford, J.A.J.; Mihara, T.; Negoro, H.; Kawai, N.; Dai, S.; Lower, M.E.; Johnston, S.; Bailes, M.; et al. The 2018 X-Ray and Radio Outburst of Magnetar XTE J1810-197. *Astrophys. J. Lett.* **2019**, *874*, L25. [CrossRef]

55. Levin, L.; Lyne, A.G.; Desvignes, G.; Eatough, R.P.; Karuppusamy, R.; Kramer, M.; Mickaliger, M.; Stappers, B.W.; Weltevrede, P. Spin frequency evolution and pulse profile variations of the recently re-activated radio magnetar XTE J1810-197. *Mon. Not. R. Astron. Soc.* **2019**, *488*, 5251–5258. [CrossRef]

56. Huang, Z.P.; Yan, Z.; Shen, Z.Q.; Tong, H.; Yuan, J.P.; Lin, L.; Zhao, R.B.; Wu, Y.J.; Liu, J.; Wang, R.; et al. Simultaneous 2.25/8.60 GHz Observations of the Magnetar XTE J1810-197. *Astrophys. J.* **2023**, *956*, 93. [CrossRef]

57. Rankin, J.M. Toward an empirical theory of pulsar emission. VI. The geometry of the conal emission region. *Astrophys. J.* **1993**, *405*, 285–297. [CrossRef]

58. Lyne, A.G.; Manchester, R.N. The shape of pulsar radio beams. *Mon. Not. R. Astron. Soc.* **1988**, *234*, 477–508. [CrossRef]

59. Wang, H.G.; Pi, F.P.; Zheng, X.P.; Deng, C.L.; Wen, S.Q.; Ye, F.; Guan, K.Y.; Liu, Y.; Xu, L.Q. A Fan Beam Model for Radio Pulsars. I. Observational Evidence. *Astrophys. J.* **2014**, *789*, 73. [CrossRef]

60. Rankin, J.M. Toward an Empirical Theory of Pulsar Emission. III. Mode Changing, Drifting Subpulses, and Pulse Nulling. *Astrophys. J.* **1986**, *301*, 901. [CrossRef]

61. Zhao, R.S.; Wu, X.J.; Yan, Z.; Shen, Z.Q.; Manchester, R.N.; Qiao, G.J.; Xu, R.X.; Wu, Y.J.; Zhao, R.B.; Li, B.; et al. TMRT Observations of 26 Pulsars at 8.6 GHz. *Astrophys. J.* **2017**, *845*, 156. [CrossRef]

62. Zhao, R.S.; Yan, Z.; Wu, X.J.; Shen, Z.Q.; Manchester, R.N.; Liu, J.; Qiao, G.J.; Xu, R.X.; Lee, K.J. 5.0 GHz TMRT Observations of 71 Pulsars. *Astrophys. J.* **2019**, *874*, 64. [CrossRef]

63. Maron, O.; Serylak, M.; Kijak, J.; Krzeszowski, K.; Mitra, D.; Jessner, A. Pulse-to-pulse flux density modulation from pulsars at 8.35 GHz. *Astron. Astrophys.* **2013**, *555*, A28. [CrossRef]

64. Xu, H.; Huang, Y.X.; Burgay, M.; Champion, D.; Cognard, I.; Guillemot, L.; Jang, J.; Karuppusamy, R.; Kramer, M.; Lackeos, K.; et al. A sustained pulse shape change in PSR J1713+0747 possibly associated with timing and DM events. *Astron. Telegr.* **2021**, *14642*, 1.

65. Wang, X.W.; Yan, Z.; Shen, Z.Q.; Tong, H.; Zhou, X.; Zhao, R.B.; Wu, Y.J.; Huang, Z.P.; Wang, R.; Liu, J. Observations of nine millisecond pulsars at 8600 MHz using the TMRT. *Astrophys. J.* **2023**, *961*, 48. [CrossRef]

66. Lu, J.G.; Du, Y.J.; Hao, L.F.; Yan, Z.; Liu, Z.Y.; Lee, K.J.; Qiao, G.J.; Shang, L.H.; Wang, M.; Xu, R.X.; et al. Multi-frequency Radio Profiles of PSR B1133+16: Radiation Location and Particle Energy. *Astrophys. J.* **2016**, *816*, 76. [CrossRef]

67. Shang, L.H.; Xu, X.; Dang, S.J.; Zhi, Q.J.; Bai, J.T.; Zhu, R.H.; Lin, Q.W.; Yang, H. A Simulation of Radius-frequency Mapping for PSR J1848-0123 with an Inverse Compton Scattering Model. *Astrophys. J.* **2021**, *916*, 62. [CrossRef]

68. Weltevrede, P.; Wright, G.A.E.; Stappers, B.W.; Rankin, J.M. The bright spiky emission of pulsar B0656+14. *Astron. Astrophys.* **2006**, *458*, 269–283. [CrossRef]

69. Yan, Z.; Shen, Z.Q.; Manchester, R.N.; Ng, C.Y.; Weltevrede, P.; Wang, H.G.; Wu, X.J.; Yuan, J.P.; Wu, Y.J.; Zhao, R.B.; et al. Simultaneous 13 cm/3 cm Single-pulse Observations of PSR B0329+54. *Astrophys. J.* **2018**, *856*, 55. [CrossRef]

70. Wen, Z.G.; Yuen, R.; Wang, N.; Tu, Z.Y.; Yan, Z.; Yuan, J.P.; Yan, W.M.; Chen, J.L.; Wang, H.G.; Shen, Z.Q.; et al. Observations of Bright Pulses from Pulsar B0031-07 at 4.82 GHz. *Astrophys. J.* **2021**, *918*, 57. [CrossRef]

71. Stinebring, D.R.; Smirnova, T.V.; Hankins, T.H.; Hovis, J.S.; Kaspi, V.M.; Kempner, J.C.; Myers, E.; Nice, D.J. Five Years of Pulsar Flux Density Monitoring: Refractive Scintillation and the Interstellar Medium. *Astrophys. J.* **2000**, *539*, 300–316. [CrossRef]

72. Scheuer, P.A.G. Amplitude variations of pulsed radio sources. *Nature* **1968**, *218*, 920–922. [CrossRef]

73. Rickett, B.J. Frequency structure of pulsar intensity fluctuations. *Nature* **1969**, *221*, 158–159. [CrossRef]

74. Anderson, B.; Lyne, A.G.; Peckham, R.J. Proper Motions of Six Pulsars. *Nature* **1975**, *258*, 215–217. [CrossRef]

75. Brouw, W.N.; Spoelstra, T.A.T. Linear polarization of the galactic background at frequencies between 408 and 1411 MHz. Reductions. *Astron. Astrophys. Suppl. Ser.* **1976**, *26*, 129–146.

76. Bartel, N.; Ratner, M.I.; Shapiro, I.I.; Cappallo, R.J.; Rogers, A.E.E.; Whitney, A.R. Pulsar Astrometry via VLBI. *Astron. J.* **1985**, *90*, 318–325. [CrossRef]

77. Fomalont, E.B.; Goss, W.M.; Beasley, A.J.; Chatterjee, S. Sub-Milliarcsecond Precision of Pulsar Motions: Using In-Beam Calibrators with the VLBA. *Astron. J.* **1999**, *117*, 3025–3030. [CrossRef]

78. Brisken, W.F.; Benson, J.M.; Goss, W.M.; Thorsett, S.E. Very Long Baseline Array Measurement of Nine Pulsar Parallaxes. *Astrophys. J.* **2002**, *571*, 906–917. [CrossRef]

79. Deller, A.T.; Tingay, S.J.; Bailes, M.; West, C. DiFX: A Software Correlator for Very Long Baseline Interferometry Using Multiprocessor Computing Environments. *Publ. Astron. Soc. Pac.* **2007**, *119*, 318–336. [CrossRef]

80. Yan, Z.; Shen, Z.Q.; Yuan, J.P.; Wang, N.; Rottmann, H.; Alef, W. Very long baseline interferometry astrometry of PSR B1257+12, a pulsar with a planetary system. *Mon. Not. R. Astron. Soc.* **2013**, *433*, 162–169. [CrossRef]